Competing exchange interactions in multiferroic and ferrimagnetic $CaBaCo_4O_7$

R. S. Fishman,[1] S. Bordács,[2] V. Kocsis,[2] I. Kézsmárki,[2] J. Viirok,[3] U. Nagel,[3] T. Rõõm,[3] A. Puri,[4] U. Zeitler,[4] Y. Tokunaga,[5,6] Y. Taguchi,[5] and Y. Tokura[5,7]

[1]*Materials Science and Technology Division, Oak Ridge National Laboratory, Oak Ridge, Tennessee 37831, USA*

[2]*Department of Physics, Budapest University of Technology and Economics and MTA-BME Lendület Magneto-optical Spectroscopy Research Group, 1111 Budapest, Hungary*

[3]*National Institute of Chemical Physics and Biophysics, Akadeemia tee 23, 12618 Tallinn, Estonia*

[4]*High Field Magnet Laboratory (HFML-EMFL), Radboud University Nijmegen, Toernooiveld 7, 6525 ED Nijmegen, The Netherlands*

[5]*RIKEN Center for Emergent Matter Science (CEMS), Wako, Saitama 351-0198, Japan*

[6]*Department of Advanced Materials Science, University of Tokyo, Kashiwa 277-8561, Japan*

[7]*Department of Applied Physics, University of Tokyo, Hongo, Tokyo 113-8656, Japan*

(Received 19 August 2016; revised manuscript received 19 December 2016; published 23 January 2017)

Competing exchange interactions can produce complex magnetic states together with spin-induced electric polarizations. With competing interactions on alternating triangular and kagome layers, the swedenborgite $CaBaCo_4O_7$ may have one of the largest measured spin-induced polarizations of $\sim$1700 nC/cm^2 below its ferrimagnetic transition temperature at 70 K. Upon rotating our sample about $\mathbf{c} = [0,0,1]$ while the magnetic field is fixed along [1,0,0], the threefold splitting of the spin-wave frequencies indicates that our sample is hexagonally twinned. Magnetization measurements then suggest that roughly 20% of the sample is in a domain with the a axis along [1,0,0] and that 80% of the sample is in one of two other domains with the a axis along either $[-1/2,\sqrt{3}/2,0]$ or $[-1/2,-\sqrt{3}/2,0]$. Powder neutron-diffraction data, magnetization measurements, and terahertz (THz) absorption spectroscopy reveal that the complex spin order in each domain can be described as a triangular array of bitetrahedral c-axis chains ferrimagnetically coupled to each other in the ab plane. The electric-field dependence of bonds coupling those chains produces the large spin-induced polarization of $CaBaCo_4O_7$.

DOI: 10.1103/PhysRevB.95.024423

I. INTRODUCTION

Competing exchange interactions produce complex magnetic states with a wide range of interesting behavior found in spin glass [1], spin ice [2], and magnetic skyrmions [3]. In multiferroic materials, complex spin states can exibit a spin-induced electric polarization **P** due to either the spin current, p-d orbital hybridization, or magnetostriction [4,5]. Because the coupling between the electrical and magnetic properties in multiferroic materials is both scientifically and technologically important, the effects of competing exchange interactions have been investigated in a wide range of multiferroic materials such as $R\mathrm{MnO_3}$ (R is a rare-earth element) [6], $\mathrm{CoCr_2O_4}$ [7], $\mathrm{CuCrO_2}$ [8], $\mathrm{CuFeO_2}$ [9], and $\mathrm{MnWO_4}$ [10]. While the first four materials [6–9] are geometrically frustrated due to competing interactions on a triangular lattice, $\mathrm{MnWO_4}$ [10] exhibits long-range competing interactions [11] on a highly-distorted monoclinic lattice.

Compounds in the "114" swedenborgite family [12] $R\mathrm{Ba}M_4\mathrm{O_7}$ (M= Co or Fe) contain alternating triangular and kagome layers, both of which are geometrically frustrated when undistorted. The "114" cobaltites [13–15] were initially studied to find charge ordering among the Co^{2+} and Co^{3+} ions. An important member of this family, $YBaCo_4O_7$ exhibits antiferromagnetic ordering [16,17] below 110 K and diffuse scattering of neutrons [13,14] indicative of spin disorder below 60 K. The magnetic state between 110 and 60 K is stabilized by a structural transition [18] that relieves the geometric frustration. Both structural and magnetic transitions are quite sensitive to excess oxygen and no magnetic order [19,20] appears in $YBaCo_4O_{7+\delta}$ for $\delta \geqslant 0.12$. Other members of this family, $CaBaFe_4O_7$ and $YbBaCo_4O_7$ undergo structural transitions at 380 K and 175 K that stabilize antiferromagnetic states below 275 K and 80 K, respectively [21,22].

A particularly interesting "114" cobaltite, $CaBaCo_4O_7$ undergoes an orthorhombic distortion [23,24] that relieves the geometric magnetic frustration on both the kagome and triangular layers sketched in Fig. 1. Below the magnetic transition temperature $T_c = 70$ K, $CaBaCo_4O_7$ develops a very large spin-induced polarization $\sim$1700 nC/cm^2 [25], second only to the conjectured [26] spin-induced polarization $\sim$3000 nC/cm^2 of $BiFeO_3$. Also unusual, $CaBaCo_4O_7$ displays a substantial ferrimagnetic moment of about 0.9 μ_B per formula unit (f.u.) [27], which could allow magnetic control of the electric polarization. Although its ferroelectric transition is inaccessible and its permanent electric polarization is not switchable [28], applications of $CaBaCo_4O_7$ might utilize the large spin-induced polarization produced by a magnetic field just below T_c [25].

This paper examines the magnetic properties of $CaBaCo_4O_7$ based on a Heisenberg model with 12 nearest-neighbor interactions and associated anisotropies. The magnetic state of $CaBaCo_4O_7$ can be described as a triangular array of ferrimagnetically aligned, bitetrahedral c-axis chains with net moment along **b**. Competing interactions within each chain produce a noncollinear spin state. The strong electric polarization of $CaBaCo_4O_7$ below T_c is induced by the displacement of oxygen atoms surrounding bonds that couple those chains.

This paper has six sections. Section II proposes a microscopic model for $CaBaCo_4O_7$. New magnetization and optical

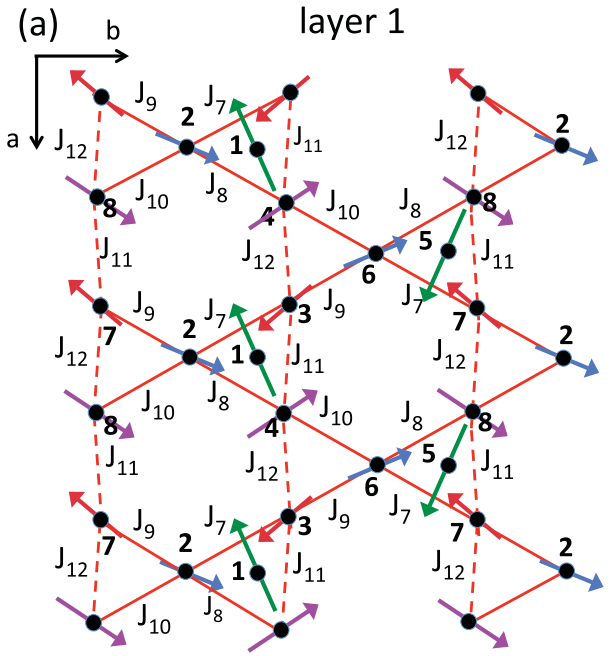

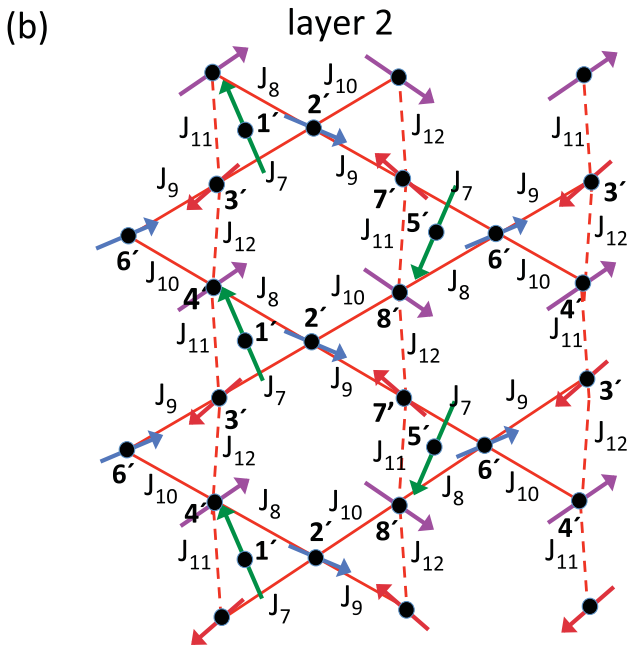

FIG. 1. (a) and (b) The predicted spin configuration for layers 1 and 2 in zero field. Spins 1 and 5 lie on a triangular layer above the first kagome layer in (a); spins 1′ and 5′ lie on a triangular layer above the second kagome layer in (b). Layers are arranged so that spins 1′ and 5′ lie directly above spins 1 and 5.

measurements are presented in Sec. III. Fitting results are discussed in Sec. IV. In Sec. V, we predict the spin-induced electric polarization. Section VI contains a conclusion.

II. MICROSCOPIC MODEL

Each magnetic unit cell of $CaBaCo_4O_7$ contains 16 Co ions on two kagome and two triangular layers with orthorhombic lattice constants $a = 6.3$ Å, $b = 11.0$ Å, and $c = 10.2$ Å. Four

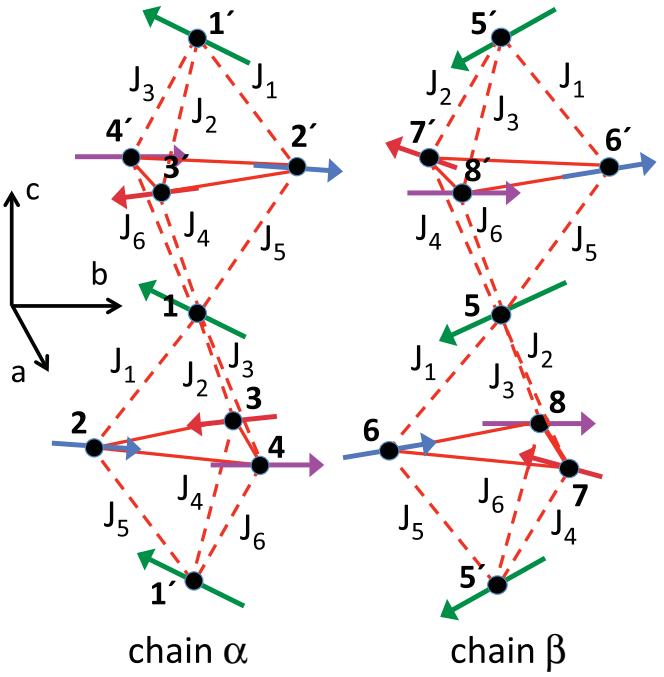

FIG. 2. A sideways view of the zero-field spin configuration showing bitetrahedral c-axis chains α and β.

crystallographically distinct Co ions have three different valences [23,29]. Triangular layers contain mixed-valent $Co^{3+}/Co^{2+}\underline{L}$ ($\underline{L}$ is a ligand hole) spins 1, 5, 9, and 13 with moments $M_1 = 2.9\,\mu_B$. Kagome layers contain Co^{2+} spins 2, 3, 6, 7, 10, 11, 14, and 15 with moments $M_2 = M_3 = 2\,\mu_B$ and mixed-valent $Co^{3+}/Co^{2+}\underline{L}$ spins 4, 8, 12, and 16 with $M_4 = 2.4\,\mu_B$. Because adjacent kagome or triangular layers are related by symmetry, $\mathbf{S}_{i'} = \mathbf{S}_{i+8}$ on layer two is identical to $\mathbf{S}_i$ on layer one. With $\mathbf{S}_i = S_i(\cos\phi_i, \sin\phi_i, 0)$ constrained to the ab plane, the ferrimagnetic moment lies along $\mathbf{b}$ if $\phi_{i+4} = \pi - \phi_i$ ($i = 1, \ldots, 4$).

The 12 different nearest-neighbor exchange couplings J_i are drawn in Figs. 1(a), 1(b), and 2. Six of these (J_1 through J_6) couple the kagome and triangular layers as shown in Fig. 2; the other six (J_7 through J_{12}) couple the spins within a kagome layer as shown in Figs. 1(a) and 1(b). The dominance of nearest-neighbor exchange over next-nearest-neighbor exchange [28] justifies setting the exchange interactions between spins on the triangular layers to zero. Our model also includes easy-plane anisotropies D, easy-axis anisotropies C within both kagome and triangular layers, and hexagonal anisotropy A on the triangular layers.

With magnetic field $\mathbf{B}$ along $\mathbf{m}$, the Hamiltonian is

$$\mathcal{H} = -\sum_{\langle i,j\rangle} J_{ij}\mathbf{S}_i\cdot\mathbf{S}_j + D^{\rm tri}\sum_{i,\rm tri} {S_{ic}}^2 + D^{\rm kag}\sum_{i,\rm kag} {S_{ic}}^2 - C^{\rm kag}\sum_{i,\rm kag}(\mathbf{o}_i\cdot\mathbf{S}_i)^2 - C^{\rm tri}\sum_{i,\rm tri}(\mathbf{n}_i\cdot\mathbf{S}_i)^2 - A^{\rm tri}\,{\rm Re}\sum_{i,\rm tri}(S_{ia}+iS_{ib})^6 - g\mu_B B\sum_i \mathbf{m}\cdot\mathbf{S}_i, \quad (1)$$

where $\mathbf{S}_i$ is a spin S operator on site i. For simplicity, we set $g = 2$ for all spins.

The easy-axis anisotropy terms proportional to $C^{\rm kag}$ and $C^{\rm tri}$ involve unit vectors $\mathbf{o}_i$ along the "bowtie" directions $\phi_i = \pi/2$ (spins 2 and 6), $5\pi/6$ (spins 3 and 8), and $7\pi/6$ (spins 4 and 7) for the kagome layers and $\mathbf{n}_i$ along the $\phi_i = \pi/6$ (spin 1) and $-\pi/6$ (spin 5) directions for the triangular layers. The hexagonal anisotropy on the triangular layers has expectation value

$$-A^{\rm tri} {S_1}^6 \sum_{i,\rm tri} \sin^6\theta_i \cos 6\phi_i .$$

All anisotropy terms may act to constrain the spins to the ab plane.

Spin amplitudes S_n are fixed at their observed values $M_n/2\mu_{\rm B}$ after performing a $1/S$ expansion about the classical limit. Alternatively, the spins S_n could all have been taken as $3/2$ but with different g factors for different sets of spins. As discussed below, that would reduce the estimated exchange coupling J_{ij} by a factor of $4S_iS_j/9$.

Static properties are obtained by minimizing the classical energy $\langle\mathcal{H}\rangle$ (the zeroth-order term in the $1/S$ expansion) with respect to the 16 spin angles. The eigenvalues and eigenvectors of a 32×32 equations-of-motion matrix [30] produced by the second-order term in the this expansion give the optical mode frequencies and absorptions, respectively.

III. MAGNETIZATION AND OPTICAL MEASUREMENTS

Perhaps due to excess or deficient oxygen [31] or different domain populations (see below), previous magnetization measurements [23,27,32–34] on $CaBaCo_4O_7$ are rather scattered. Consequently, new magnetization measurements were performed at 4 K on hexagonally twinned crystals with a common $\mathbf{c} = \mathbf{z} = [0,0,1]$ axis. In domain I, $\mathbf{a}$ lies along the laboratory direction $\mathbf{x} = [1,0,0]$ and $\mathbf{b}$ lies along $\mathbf{y} = [0,1,0]$, in domain II, $\mathbf{a} = [-1/2,\sqrt{3}/2,0]$ and $\mathbf{b} = [-\sqrt{3}/2,-1/2,0]$, and in domain III, $\mathbf{a} = [-1/2,-\sqrt{3}/2,0]$ and $\mathbf{b} = [\sqrt{3}/2,-1/2,0]$. If p_l are the domain populations, then the magnetizations M_x and M_y measured with fields along $\mathbf{x}$ and $\mathbf{y}$ only depend on p_1 and $p_2 + p_3 = 1 - p_1$. Of course, M_z measured with field along $\mathbf{z}$ is independent of p_l. Figure 3 indicates that all three magnetizations increase monotonically up to at least 32 T.

Previous optical measurements [35] at the ordering wave vector $\mathbf{Q}$ found two conventional spin-wave modes that couple to the ground state through the magnetization operator $\mathbf{M} = 2\mu_{\rm B}\sum_i \mathbf{S}_i$. These magnetic-resonance (MR) modes are degenerate in zero field with a frequency of 1.07 THz and split almost linearly with increasing field along $\mathbf{y}$, as shown in Fig. 4. For $\mathbf{m} = \mathbf{y}$, the MR modes are excited in two geometries: (i) with THz fields $\mathbf{E}_\omega||\mathbf{x}$ and $\mathbf{B}_\omega||\mathbf{z}$ and (ii) with $\mathbf{E}_\omega||\mathbf{z}$ and $\mathbf{B}_\omega||\mathbf{x}$. Those measurements also found an electromagnon (EM) that couples to the ground state through the polarization operator $\mathbf{P}$. The EM with zero-field frequency 1.41 THz is only excited in geometry ii.

Because the exchange couplings already break every degeneracy in the unit cell, the 16 predicted modes for a single domain are nondegenerate. Therefore the split MR modes must come from different domains. This was verified by measuring [36] the MR mode frequencies as a function of the rotation angle θ for field $\mathbf{B} = B(\cos\theta, \sin\theta, 0) = B(\mathbf{x}\cos\theta + \mathbf{y}\sin\theta)$ in the laboratory reference frame. In practice, this is accomplished by rotating the sample about $\mathbf{c}$ while keeping the field fixed along $\mathbf{x}$. As shown in Fig. 5 for 12 and 15 T, each hexagonal domain then contributes one MR branch with a period of π.

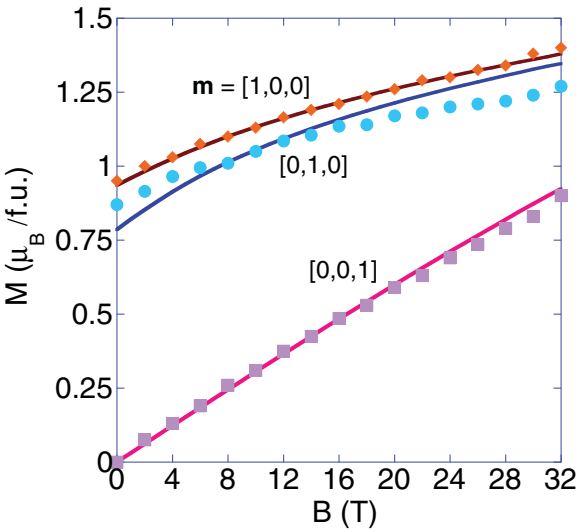

FIG. 3. The measured (symbols) and predicted (solid curves) magnetizations for field along [1,0,0], [0,1,0], or [0,0,1].

With field $\mathbf{B}_{\rm loc} = B(\cos\psi, \sin\psi, 0) = B(\mathbf{a}\cos\psi + \mathbf{b}\sin\psi)$ in the domain reference frame, the upper MR mode in Fig. 4 corresponds to the $\psi = \pi/2$ mode for domain I, while the lower MR mode corresponds to the degenerate $\psi = \pm\pi/6$ modes for domains II and III. Previously measured MR frequencies plotted in Fig. 4 at 12 T correspond to the diamond and triangular points in Fig. 5(b) at $\theta = \pi/2$. Cusps in the MR curves for each domain at $\psi = 0$ and π are caused by flipping the b component of the magnetization [see inset to Fig. 5(b)].

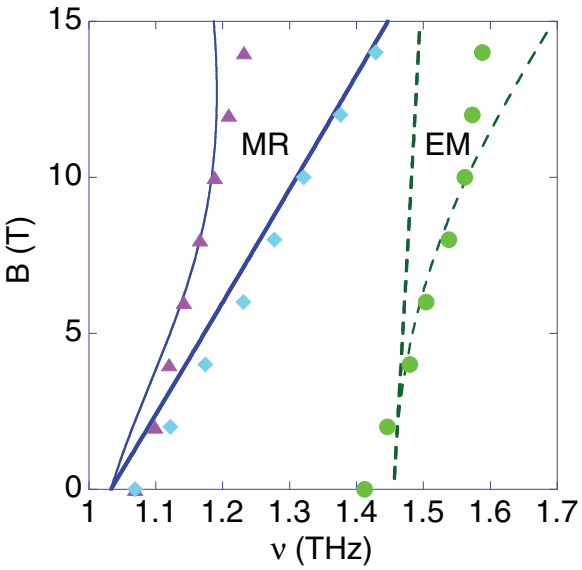

FIG. 4. The predicted MR (solid) and EM (dashed) modes for domain I (thick) and domains II and III (thin). Measured modes are indicated by symbols.

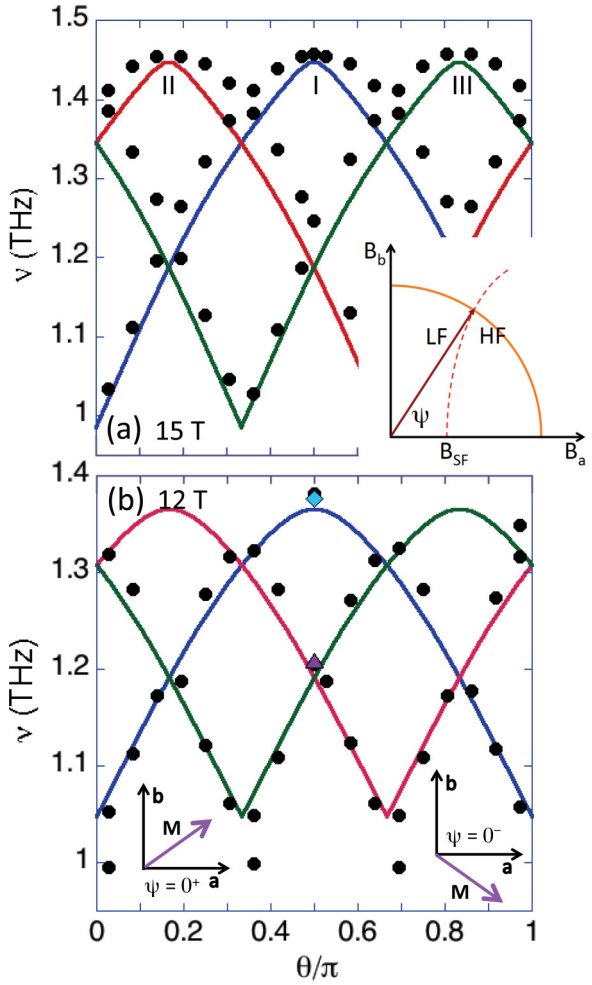

FIG. 5. The measured (solid circles) and predicted (blue, red, and green curves for domains I, II, and III, respectively) angular dependence of the MR mode frequencies for 12 and 15 T. The inset to (a) sketches the angular dependence of $\mathbf{B}_{SF}$ (dashed curve), which separates low-field (LF) and high-field (HF) states. The inset to (b) shows the net magnetization of any domain for angles ψ on either side of 0. Flips of the b-axis spin at $\psi = 0$ and π produce cusps in the mode frequencies.

IV. FITTING RESULTS

Fits for the coupling parameters utilize the field dependence of **M**, the zero-field neutron powder-diffraction data [23], the field dependence of the MR and EM modes at $\theta = \pi/2$ [35], and the MR mode frequencies at $\theta = 0$ and $\pi/3$ for 7, 12, and 15 T. The resulting exchange and anisotropy constants are provided in Table I and the corresponding zero-field spin state is plotted in Figs. 1(a) and 1(b). In contrast to the previously proposed [23] spin state with zigzag chains in the ab plane containing spins 2, 3, 6, and 7, our spin state can be better described as an array of c-axis chains or connected bitetrahedra [16,37] containing spins {1,2,3,4} (chain α) or {5,6,7,8} (chain β) as sketched in Fig. 2. Chains are coupled by exchanges J_9, J_{10}, and J_{12} in the ab plane.

What explains the wide range of J_i values? An orthorhombic distortion [23,24] with $b/(a\sqrt{3}) - 1 \to 0.018$ as $T \to 0$ breaks the hexagonal symmetry of the ab plane and explains the difference between the pairs $\{J_1, J_2\}$, $\{J_8, J_{11}\}$, and $\{J_{10}, J_{12}\}$. The difference between couplings like $\{J_7, J_8\}$ is caused by charge ordering: whereas J_7 couples moments 2 and 3 with $M_2 = M_3$, J_8 couples moments 2 and 4 with $M_2 \neq M_4$. Charge ordering also explains the difference between the pairs $\{J_2, J_3\}$ and $\{J_9, J_{10}\}$. Although not demanded by symmetry, we set $J_1 = J_5$, $J_2 = J_4$, $J_3 = J_6$, and $J_{11} = J_{12}$ because the spin state and excitations at **Q** only depend on their averages [38].

Given other conditions, our fit chooses the spin state that matches the neutron powder-diffraction data [23] as closely as possible. At zero field, the predicted spin state has angles $\phi_1 = -0.83\pi$, $\phi_2 = 0.40\pi$, $\phi_3 = -0.23\pi$, and $\phi_4 = 0.62\pi$. Based exclusively on powder-diffraction data and symmetry constraints, the previously proposed spin state [23] had $\phi_1 = -0.24\pi$, $\phi_2 = \phi_3 = 0.67\pi$, and $\phi_4 = -0.44\pi$. In both cases, $\phi_{i+4} = \pi - \phi_i$ ($i = 1, \ldots, 4$) so that the moment $\mathbf{M}_b$ lies along the b axis. As shown in Table II, our spin state does not satisfy the powder diffraction data quite as well as the earlier state, primarily because it underestimates the powder diffraction peak $I(112)$.

For the previous spin state, χ^2 is minimized by Lorentzian form factors with $Q_1/4\pi = 0.088$ Å^{-1}, $Q_2/4\pi = Q_3/4\pi = 0.095$ Å^{-1}, and $Q_4/4\pi = 0.088$ Å^{-1} for spins S_n. For the new spin state, $Q_1/4\pi = 0.052$ Å^{-1}, $Q_2/4\pi = Q_3/4\pi = 0.224$ Å^{-1}, and $Q_4/4\pi = 0.102$ Å^{-1}. Note that $Q_2/4\pi$ and $Q_3/4\pi$ are smaller than the scale $Q_0/4\pi \approx 0.3$ Å^{-1} measured by Khan and Erickson [39] for Co^{2+} in CoO.

Our results indicate that the exchange coupling $J_8 \approx 188$ meV between moments 2 (Co^{2+}, $S_2 = 1$) and 4 ($Co^{3+}/Co^{2+}\underline{L}$, $S_4 = 1.2$) is strongly ferromagnetic and larger in magnitude even than the 155 meV antiferromagnetic coupling found in the cuprate Nd_2CuO_4 [40]. The strength of this coupling might be explained by the double-exchange mediated hopping of ligand holes $\underline{L}$ [19] from site 4 to 2. Bear in mind, however, that the estimated exchange parameters would be significantly reduced if we had taken $S = 3/2$ for all Co spins. In particular, J_8 would then fall from 188 to 100 meV.

Except for J_{10}, the five largest exchange couplings $J_1 = J_5 \approx -92$ meV, $J_3 = J_6 \approx 41$ meV, and $J_8 \approx 188$ meV lie within connected bitetrahedral c-axis chains. Inside each chain, competing interactions between spins 1, 2, and 4 produce a noncollinear spin state.

TABLE I. Exchange and anisotropy parameters (mev).

	p_1	$J_1 = J_5$	$J_2 = J_4$	$J_3 = J_6$	J_7	J_8	J_9	J_{10}	$J_{11} = J_{12}$	D^{kag}	D^{tri}	C^{kag}	C^{tri}	$S_1{}^4 A^{tri}$
	0.185	−91.5	−10.8	41.4	−29.9	187.8	7.9	108.0	−6.7	−0.67	−1.24	3.70	0.77	0.0064
error	±0.071	±3.6	±0.5	±0.7	±1.9	±7.5	±0.1	±4.5	±0.1	±0.06	±0.03	±0.15	±0.09	±0.0004

TABLE II. Ratios of powder-diffraction peak intensities.

	$I(002)/I(101)$	$I(012)/I(101)$	$I(111)/I(101)$	$I(112)/I(101)$	$I(121)/I(101)$	$I(122)/I(101)$	$M_b(\mu_B$/f.u.)	χ^2
experimental [23]	0.344	0.326	0.322	0.477	0.262	0.404		
previous [23]	0.286	0.414	0.384	0.411	0.232	0.427	0.88	0.021
current	0.360	0.380	0.378	0.286	0.313	0.449	1.33	0.047

Although occupying a triangular lattice, chains α and β are magnetically ordered with moments $\mathbf{M}^{\rm ch} = (\pm 1.18, 1.33, 0)\mu_B$/f.u.. These chains are primarily coupled by the strongly ferromagnetic interaction $J_{10} \approx 108$ meV between nearly parallel spins $\{4,6\}$ ($\phi_4 = 0.62\pi, \phi_6 = 0.60\pi$) and $\{2,8\}$ ($\phi_2 = 0.40\pi$, $\phi_8 = 0.38\pi$). Above $T_c = 70$ K, the short-range order within each chain may be responsible for the large, negative Curie-Weiss temperature $\Theta_{\rm CW} \approx -1720$ [27] or -890 K [32], the larger than expected Curie constant [27], and the susceptibility anomaly [32] at 360 K suggestive of short-range magnetic order far above T_c.

Comparison between the theoretical and experimental results for the magnetization in Fig. 3 suggests that roughly 20% of the sample is in domain I. Different domain populations or even orthorhombic twinning in other samples may explain the discrepancies between the reported magnetization measurements [23,27,32–34].

Easy-axis anisotropies A and C favor ferrimagnetic alignment along **b** rather than **a**. The spin-flop (SF) field required to flip the spins towards the **a** direction must increase as the field along **b** increases [41]. As shown in the inset to Fig. 5(a), $B_{\rm SF}(\psi)$ then increases with ψ. If $B_{\rm SF}(\psi = 0) < 15$ T, then the MR spectrum for 15 T would show a discontinuity at the transition from a low-field (LF) to a high-field (HF) state below some critical value of ψ. Since the MR mode frequencies in Fig. 5(a) do not exhibit any discontinuities as a function of ψ, we conclude that $B_{\rm SF}(\psi = 0)$ exceeds 15 T and probably, based on the smooth dependence of the magnetizations on field, exceeds 32 T as well. The apparent small size of $B_{\rm SF}$ [25,42] must reflect the net magnetization of all three domains.

Predicted modes below 5 THz are plotted in Fig. 4. The Goldstone modes for all three domains are lifted by in-plane anisotropies to become the MR modes with zero-field frequencies of 1.07 THz. As remarked earlier, the lower MR mode comes from domains II and III while the upper MR mode comes from domain I. Below 3.5 THz, one EM mode is produced in domain I and another in domains II and III. The degenerate EM modes from domains II and III dominate the optical absorption. The predicted field dependence of the upper MR mode is quite close to the observed dependence. However, the predicted curvatures of the lower MR and the EM modes, both from domains II and III, is not observed.

V. SPIN-INDUCED ELECTRIC POLARIZATION

Below the ferrimagnetic transition, $CaBaCo_4O_7$ is reported [25] to develop a very large spin-induced polarization $\sim$1700 nC/cm^2, which is surpassed in type-I multiferroics only by the conjectured [26] spin-induced polarization $\sim$3000 nC/cm^2 of $BiFeO_3$. Other measurements indicate that the spin-induced polarization of $CaBaCo_4O_7$ ranges from 320 nC/cm^2 [33] to 900 nC/cm^2 [43].

The electric-field dependence of any interaction term in the spin Hamiltonian $\mathcal{H}$ can induce an electric polarization below T_c. However, the electric-field dependence of the easy-plane anisotropy D cannot explain the spin-induced polarization along **c** because the expectation value of $P_i = \kappa {S_{ic}}^2$ with $\kappa = -\partial D/\partial E_c$ would vanish in zero magnetic field when all the spins lie in the ab plane. Easy-axis anisotropy A or C in the ab plane could produce a spin-induced electric polarization perpendicular to **c**. But the EM mode would then become observable for a THz electric field in the ab plane, contrary to measurements.

As conjectured previously [25], the spin-induced polarization in $CaBaCo_4O_7$ must then be generated by the dependence of the exchange interactions J_{ij} on an electric field, called magnetostriction. Coupling constant $\lambda_{ij} = \partial J_{ij}/\partial E_c$ for bond $\{i,j\}$ is associated with a spin-induced polarization [44] per site of $P_c^{ij} = \lambda_{ij}\, \mathbf{S}_i \cdot \mathbf{S}_j/4$, which accounts for the four equivalent bonds per unit cell. Expanding in the electric field E_c yields an interaction term $-E_c\, \lambda_{ij}\, \mathbf{S}_i \cdot \mathbf{S}_j$, linear in the electric field and quadratic in the spin operators.

Taking $|0\rangle$ as the ground state and $|n\rangle$ as the excited spin-wave state, the MR matrix element $\langle n|M_a|0\rangle$ mixes with the EM matrix element $\langle n|P_c^{ij}|0\rangle$ for domains II and III but not for domain I. Therefore our model can explain the strong asymmetry [45] $\sim$Re$\{\langle n|\mathbf{M}\cdot\mathbf{B}_\omega|0\rangle\langle 0|\mathbf{P}\cdot\mathbf{E}_\omega|n\rangle\}$ in the absorption of counter-propagating light waves [35] for the lower observed MR mode in geometry ii with $\mathbf{E}_\omega||\mathbf{c}$. However, it cannot explain the observed asymmetry of this mode in geometry i with $\mathbf{E}_\omega \perp \mathbf{c}$ if only $\langle 0|P_c|n\rangle$ is significant.

How can we estimate the coupling constants λ_{ij} and the spin-induced electric polarization? The optical absorption of any mode in domain l is proportional to p_l. So at nonzero field, the EM absorption is proportional to $p_2 + p_3 = 1 - p_1$ while the upper MR mode absorption is proportional to p_1. At zero field, all domains have the same mode spectrum so that both the MR and EM mode absorptions are proportional to $p_1 + p_2 + p_3 = 1$. Experimentally, the ratio r of the absorption of the EM mode to the absorption of the upper MR mode rises from $r = 7.5$ at 0 T to $r = 35$ at 10 T. This growth is explained by the $B > 0$ ratio $(1 - p_1)/p_1 = 4.4$.

At both 0 and 10 T, the only sets of bonds that generate spin-induced polarizations of the right magnitude are $\{2,7\}$ and $\{3,4\}$. Each of those bonds couples adjacent c-axis chains through pairs of spins that are almost antiparallel. From the relative absorptions r at 0 or 10 T, we estimate that $\langle P_c^{27}\rangle \approx 2350$ or 2920 nC/cm^2 and $\langle P_c^{34}\rangle \approx 2110$ or 2570 nC/cm^2. Results for both sets of bonds are consistent with the recently observed [25] polarization of 1700 nC/cm^2. By contrast, density-functional theory [28] predicts that the spin-induced polarization along **c** is 460 nC/cm^2. The spin-induced polarization should remain fairly constant with

applied magnetic field, decreasing by about 1% for a 10 T field along **b**.

VI. CONCLUSION

We have presented a nearly complete solution for the magnetization, spin state, and mode frequencies of the swedenborgite $CaBaCo_4O_7$. An orthorhombic distortion above T_c partially relieves the geometric frustration on the kagome and triangular layers and allows ferrimagnetism and ferroelectricity to coexist below T_c. Although occupying a triangular lattice, bitetrahedral c-axis chains are ferrimagnetically ordered in the ab plane. Competing interactions within each chain produce noncollinear spin states. Sets of bonds coupling those chains are responsible for the large spin-induced polarization of $CaBaCo_4O_7$.

Despite its fixed permanent electric polarization, this swedenborgite may yet have important technological applications utilizing the large changes [25] in the spin-induced polarization when a modest magnetic field below 1 T is applied along **b** in the vicinity of T_c. A big jump in the polarization should also be produced just below T_c by rotating a fixed magnetic field about the c axis. Above all, our work illuminates a pathway to develop other functional materials with sizable magnetic moments and electrical polarizations.

ACKNOWLEDGMENTS

Research sponsored by the U.S. Department of Energy, Office of Science, Basic Energy Sciences, Materials Sciences and Engineering Division (RF), by the Hungarian Research Funds OTKA K 108918, OTKA PD 111756, and Bolyai 00565/14/11 (SB, VK, and IK), by the institutional research funding IUT23-3 of the Estonian Ministry of Education and Research and the European Regional Development Fund project TK134 (TR and UN), and by the Funding Program for World-Leading Innovative R&D on Science and Technology (FIRST Program) (YT, YT, and YT). We also acknowledge the support of the HFML-RU/FOM, member of the European Magnetic Field Laboratory (EMFL).

This manuscript has been authored by UT-Battelle, LLC under Contract No. DE-AC05-00OR22725 with the U.S. Department of Energy. The United States Government retains and the publisher, by accepting the article for publication, acknowledges that the United States Government retains a nonexclusive, paid-up, irrevocable, world-wide license to publish or reproduce the published form of this manuscript, or allow others to do so, for United States Government purposes. The Department of Energy will provide public access to these results of federally sponsored research in accordance with the DOE Public Access Plan (http://energy.gov/downloads/doe-public-access-plan).

[1] K. Binder and A. P. Young, Rev. Mod. Phys. **58**, 801 (1986).
[2] M. J. Harris, S. T. Bramwell, D. F. McMorrow, T. Zeiske, and K. W. Godfrey, Phys. Rev. Lett. **79**, 2554 (1997).
[3] S. Mühlbauer, B. Binz, F. Jonietz, C. Pfleiderer, A. Rosch, A. Neubauer, R. Georgii, and P. Böni, Science **323**, 915 (2009).
[4] D. I. Khomskii, J. Magn. Magn. Mater. **306**, 1 (2006).
[5] S.-W. Cheong and M. Mostovoy, Nat. Mat. **6**, 13 (2007).
[6] A. B. Sushkov, R. V. Aguilar, S. Park, S.-W. Cheong, and H. D. Drew, Phys. Rev. Lett. **98**, 027202 (2007).
[7] Y. Yamasaki, S. Miyasaka, Y. Kaneko, J.-P. He, T. Arima, and Y. Tokura, Phys. Rev. Lett. **96**, 207204 (2006).
[8] M. Soda, K. Kimura, T. Kimura, and K. Hirota, Phys. Rev. B **81**, 100406 (2010).
[9] S. Seki, N. Kida, S. Kumakura, R. Shimano, and Y. Tokura, Phys. Rev. Lett. **105**, 097207 (2010).
[10] K. Taniguchi, N. Abe, S. Ohtani, and T. Arima, Phys. Rev. Lett. **102**, 147201 (2009).
[11] F. Ye, R. S. Fishman, J. A. Fernandez-Baca, A. A. Podlesnyak, G. Ehlers, H. A. Mook, Y.-Q. Wang, B. Lorenz, and C. W. Chu, Phys. Rev. B **83**, 140401 (2011).
[12] B. Raveau, V. Caignaert, V. Pralong, and A. Maignan, Z. Anorg. Allg. C **635**, 1869 (2009).
[13] M. Valldor and M. Andersson, Sol. St. Sci. **4**, 923 (2002); M. Valldor, *ibid.* **6**, 251 (2004).
[14] E. V. Tsipis, D. D. Khalyavin, S. V. Shiryaev, K. S. Redkina, and P. Núñez, Mat. Chem. Phys. **92**, 33 (2005); E. V. Tsipis, V. V. Kharton, J. R. Frade, and P. Núñez, J. Sol. St. Electrochem. **9**, 547 (2005).
[15] G. L. Bychkov, S. N. Barilo, S. V. Shiryaev, D. V. Sheptyakov, S. N. Ustinovich, A. Podlesnyak, M. Baran, R. Szymczak, and A. Furrer, J. Cryst. Growth **275**, e813 (2005).
[16] L. C. Chapon, P. G. Radaelli, H. Zheng, and J. F. Mitchell, Phys. Rev. B **74**, 172401 (2006).
[17] D. D. Khalyavin, P. Manuel, B. Ouladdiaf, A. Huq, P. W. Stephens, H. Zheng, J. F. Mitchell, and L. C. Chapon, Phys. Rev. B **83**, 094412 (2011).
[18] A. K. Bera, S. M. Yusuf, and S. Banerjee, Sol. St. Sci. **16**, 57 (2013).
[19] A. Maignan, V. Caignaert, D. Pelloquin, S. Hébert, V. Pralong, J. Hejtmanek, and D. Khomskii, Phys. Rev. B **74**, 165110 (2006).
[20] S. Avci, O. Chmaissem, H. Zheng, A. Huq, P. Manuel, and J. F. Mitchell, Chem. Mat. **25**, 4188 (2013).
[21] A. Huq, J. F. Mitchell, H. Zheng, L. C. Chapon, P. G. Radaelli, K. S. Knight, and P. W. Stephens, J. Sol. St. Chem. **179**, 1136 (2006).
[22] V. Kocsis, Y. Tokunaga, S. Bordács, M. Kriener, A. Puri, U. Zeitler, Y. Taguchi, Y. Tokura, and I. Kézsmárki, Phys. Rev. B **93**, 014444 (2016).
[23] V. Caignaert, V. Pralong, V. Hardy, C. Ritter, and B. Raveau, Phys. Rev. B **81**, 094417 (2010).
[24] S. N. Panja, J. Kumar, S. Dengre, and S. Nair, J. Phys.: Cond. Mat. **16**, 9209 (2016).
[25] V. Caignaert, A. Maignan, K. Singh, Ch. Simon, V. Pralong, B. Raveau, J. F. Mitchell, H. Zheng, A. Huq, and L. C. Chapon, Phys. Rev. B **88**, 174403 (2013).
[26] J.-H. Lee and R. S. Fishman, Phys. Rev. Lett. **115**, 207203 (2015).
[27] V. Caignaert, V. Pralong, A. Maignon, and B. Raveau, Sol. St. Comm. **149**, 453 (2009).
[28] R. D. Johnson, K. Cao, F. Giustino, and P. G. Radaelli, Phys. Rev. B **90**, 045129 (2014).

[29] S. Chatterjee and T. Saha-Dasgupta, Phys. Rev. B **84**, 085116 (2011).
[30] R. S. Fishman, J. T. Haraldsen, N. Furukawa, and S. Miyahara, Phys. Rev. B **87**, 134416 (2013).
[31] Md. M. Seikh, V. Caignaert, V. Pralong, and B. Raveau, J. Phys. Chem. Sol. **75**, 79 (2014).
[32] Z. Qu, L. Ling, L. Zhang, and Y. Zhang, Sol. St. Comm. **151**, 917 (2011).
[33] H. Iwamoto, M. Ehara, M. Akaki, and H. Kuwahara, J. Phys.: Conf. Ser. **400**, 032031 (2012).
[34] Md. Motin Seikh, T. Sarkar, V. Pralong, V. Caignaert, and B. Raveau, Phys. Rev. B **86**, 184403 (2012).
[35] S. Bordács, V. Kocsis, Y. Tokunaga, U. Nagel, T. Rõõm, Y. Takahashi, Y. Taguchi, and Y. Tokura, Phys. Rev. B **92**, 214441 (2015).
[36] The THz spectra of $CaBaCo_4O_7$ were measured at 2.5 K with linear light polarization using Fourier-transform spectroscopy [35]. The reference spectrum was taken in zero field.
[37] M. Valldor, J. Phys.: Cond. Mat. **16**, 9209 (2004).
[38] Spin excitations away from $\mathbf{q} = \mathbf{Q}$ depend separately on these exchange constants. The stability of the coplanar ground state requires that each pair of exchange constants be sufficiently close to one another.
[39] D. C. Khan and R. A. Erickson, Phys. Rev. B **1**, 2243 (1970).
[40] P. Bourges, H. Casalta, A. S. Ivanov, and D. Petitgrand, Phys. Rev. Lett. **79**, 4906 (1997).
[41] While the coplanar LF spin state has a lower energy than the HF state below 32 T, it becomes locally unstable to a buckled state with spins canted out of the ab plane between 16 and 32 T for field along **a**. Based on the smooth dependence of the magnetizations on field, the transition from the coplanar to the buckled state must be second order.
[42] V. Pralong, V. Caignert, T. Sarkar, O. I. Lebedev, V. Duffort, and B. Raveau, J. Sol. St. Chem. **184**, 2588 (2011).
[43] V. Kocsis, S. Bordács, and I. Kézsmárki (unpublished).
[44] Based on the symmetry of adjacent layers, it is easy to show that the polarization operator $\mathbf{P}^{12}$ associated with bond {1,2} has components

$$P_a^{12} \propto C_{12} - C_{56} - C_{1'2'} + C_{5'6'},$$
$$P_b^{12} \propto C_{12} + C_{56} - C_{1'2'} - C_{5'6'},$$
$$P_c^{12} \propto C_{12} + C_{56} + C_{1'2'} + C_{5'6'},$$

where $C_{ij} = \mathbf{S}_i \cdot \mathbf{S}_j$. Similar relations hold for other bonds. Only the c component P_c^{ij} can produce a static polarization but all three components may contribute to the off-diagonal polarization matrix elements $\langle 0|P_\alpha^{ij}|n\rangle$ $(n \neq 0)$.
[45] S. Miyahara and N. Furukawa, J. Phys. Soc. Japan **80**, 073708 (2011).